Automotive radar interference study for different radar waveform types

Kumbul, Utku; Uysal, Faruk; Vaucher, Cicero S.; Yarovoy, Alexander

DOI
10.1049/rsn2.12203

Publication date
2021

Document Version
Final published version

Published in
IET Radar, Sonar and Navigation

Received: 25 June 2021 | Revised: 21 October 2021 | Accepted: 14 November 2021

IET Radar, Sonar & Navigation

DOI: 10.1049/rsn2.12203

The Institution of Engineering and Technology WILEY

ORIGINAL RESEARCH

Automotive radar interference study for different radar waveform types

Utku Kumbul[1] | Faruk Uysal[1] | Cicero S. Vaucher[1,2] | Alexander Yarovoy[1]

[1]Department of Microelectronics, Delft University of Technology, Delft, The Netherlands

[2]NXP Semiconductors, Eindhoven, The Netherlands

Correspondence

Utku Kumbul, Department of Microelectronics, Delft University of Technology, Building 36, Mekelweg 4, 2628 CD Delft, The Netherlands.
Email: u.kumbul@tudelft.nl

Funding information

NXP Semiconductors N.V. and Holland High Tech Systems and Materials, Grant/Award Number: TKI-HTSM/18.0136

Abstract

Mutual interference between different radar waveforms used in automotive radar applications is studied. The existing interference analysis is extended to a generalised radar-to-radar interference equation that covers most of the common interference scenarios for automotive radar systems. The outcome of the generalised equation is demonstrated for a number of typical scenarios where radars with different continuously transmitting waveforms are involved. The proposed equation can be used to characterise the received interference and its features by analysing the instantaneous beat frequency of the victim radar. Moreover, an interference analysis of phase-coded frequency-modulated continuous waveforms is performed and demonstrated experimentally by using real-time automotive radars for the first time in the literature. The experimental results corroborate the interference analysis of different waveforms and validate the proposed generalised interference equation under various conditions.

KEYWORDS

automotive radar, phase coding, radar interference, waveform analysis

1 | INTRODUCTION

Radar systems are widely used in defence, meteorology, surveillance, medicine and automotive systems. The increasing number of radars on the roads raises safety concerns regarding radar-to-radar interference in automotive systems [1]. Multiple radars operating simultaneously within the same frequency bandwidth cause mutual interference [2]. In general, there are three types of interference: (1) self-interference, caused by a strong return signal reflected by the platform (the radome or the bumper) or the coupling (spill-over) effect between transmitter and receiver; (2) cross-interference caused by multiple transceivers on the same vehicle, or within the same transceiver such as with a multiple input multiple output (MIMO) system; and (3) interference caused by other radars in the vicinity [3]. Interference of any kind downgrades the detection capability and functionality of the radar system that is being interfered with, known as the 'victim radar' [3–6]. Consequently, various studies have been conducted on mitigating interference, using approaches with different processing costs and hardware complexity [7–10]. However, the structure of the interference varies according to the radar waveform type. Therefore, it is important to analyse different interference scenarios for various modulation schemes.

The frequency-modulated continuous waveform (FMCW) has been one of the most often used modulation schemes for automotive radar application in the past few decades [3]. This modulation scheme transmits continuous waveforms that have linearly changing frequencies. One of the main advantages of FMCW is stretch processing (also known as dechirping or deramping) to reduce the waveform sampling requirements of the radar receiver. During the dechirping process, the received and transmitted signals are mixed and low-pass filtered (LPF) to obtain a baseband signal. The frequency of the baseband signal (beat signal) contains information on the range and velocity of the targets [11]. For the traditional FMCW radar, bursts with different pulse repetition frequencies (PRF) are used to cope with ambiguities and to discriminate between multiple targets [12]. Modern radars use chirp sequencing, which allows for the processing of range and Doppler information by using a two-dimensional Fourier transform [13].

Another well-known modulation scheme is the phase-modulated continuous waveform (PMCW). In the PMCW,

the transmitted signal is modulated by changing the phase of the waveform. This phase change is controlled by a code sequence, and for that reason the phase modulation is also called phase coding (PC) or pseudo-noise (PN) sequencing [14]. The received signal is down-converted to the baseband, and the baseband signal is correlated with the complex conjugate of the transmitted code sequence [15]. Several code families have been studied in the literature, including binary code sequences [16] and poly-phase codes [17–19]. Depending on the code selection and design, low cross-correlation and low-range side lobes can be achieved [20]. The optimal code selection varies with the requirement of the application.

Recently, there has been growing interest in the phase-coded frequency-modulated continuous waveform (PC-FMCW) radar [21–23]. The idea of using phase coding for FMCW enables radar-communication (RadCom) coexistence [24]. Moreover, the PC-FMCW enhances mutual orthogonality between waveforms and can be used for interference mitigation [25]. In [21], the PC-FMCW signal is processed by the matched filter, where the received signal is convolved with the complex conjugate of the transmitted signal. However, the traditional matched filtering operation in the digital domain requires a high sampling rate from the receiver since the full bandwidth of the transmitted signal is needed. Thus, it is difficult to realise a matched filtering strategy given the limited hardware and processing power of automotive radars that have a chirp bandwidth of maximally 4 GHz. Instead of matched filtering, the dechirping and decoding strategy is therefore adapted for the PC-FMCW radar to decrease the sampling requirement of the receiver. This dechirping and decoding strategy requires the alignment of beat signals in order to achieve proper decoding. Alignment of the beat signals is achieved by using an ideal group delay filter in [25, 26]. After decoding, the beat signals obtained are similar to conventional FMCW and hence the target information can be extracted by applying spectral estimation techniques.

In this article we focus on mutual interference between the victim radar and the interfering sensor with various types of continuous waveform. The automotive radar interference of different radar waveforms is investigated analytically. We derive a generalised radar-to-radar interference equation to describe the appearance of the interference at the beat (intermediate) frequency. The derived equation converges to some specific cases in the literature and additionally it includes interference analysis of phase-coded waveforms. We consider the PC-FMCW radar as a general case and investigate the instantaneous beat frequency of the victim radar to understand the features of the interference. Consequently, the different interference types can be directly obtained and adequately simulated by using the proposed equation. Thus, the outcome of this equation allows for a detailed analysis regarding the impacts of different interference types on target detection. In addition, the experiments are conducted by using the commercially available off-the-shelf automotive radar transceivers and the experimental verification of the proposed generalised interference equation is demonstrated for different scenarios.

The rest of the study is organised as follows. Section 2 gives useful background information and describes the signal models for the waveforms. Section 3 presents the convergence of the generalised interference equation with other studies in the literature. Section 4 provides verification of the experiments and discusses the utilisation of the proposed equation, while Section 5 offers further discussion on some of the relevant topics. Finally, Section 6 highlights the concluding remarks.

2 | BACKGROUND AND SIGNAL MODEL

This section describes the signal models for common automotive radar waveforms (as illustrated in Figure 1) and introduces the generalised radar-to-radar interference equation for those waveforms.

The transmitted signal for continuous waveform (CW) radar can be represented as:

$$x_{t_{CW}}(t) = \sqrt{P_t}\exp\left(j2\pi f_c t\right), \tag{1}$$

where P_t is the power of the transmitted signal and f_c is the carrier frequency. The transmitted signal for FMCW can be represented as:

$$x_{t_{FMCW}}(t) = \sqrt{P_t}\exp\left(j2\pi\left(f_c t + \frac{1}{2}kt^2\right)\right), \tag{2}$$

where k is the slope of the linear frequency modulated waveform and is equal to the ratio of bandwidth and sweep duration, described as $k = B/T$. The transmitted signal for PMCW can be represented as:

$$x_{t_{PMCW}}(t) = c_t(t)\sqrt{P_t}\exp\left(j2\pi f_c t\right), \tag{3}$$

where $c_t(t)$ is a single period of a transmitted phase code. Note that the phase code can also be written as a phase term inside the exponent. Since we would like to generalise the equation, we prefer to keep the phase coding term as a separate signal component. In PC-FMCW radar [25], both the frequency and phase of the transmitted signal change over time. The transmitted signal for a phase-coded FMCW radar can be written as:

$$x_{t_{PC-FMCW}}(t) = c_t(t)\sqrt{P_t}\exp\left(j2\pi\left(f_c t + \frac{1}{2}kt^2\right)\right) \tag{4}$$

For simplicity we represent the coding signal mathematically by using a phase term, as follows:

$$c_t(t) = \sum_{n=1}^{L_a} e^{j\phi_n}\mathrm{rect}\left(\frac{t-(n-1/2)T_a}{T_a}\right), \tag{5}$$

where L_a is the number of chips within one sweep, T_a is the single-chip duration, calculated as $T_a = T/L_a$ and ϕ_n denotes

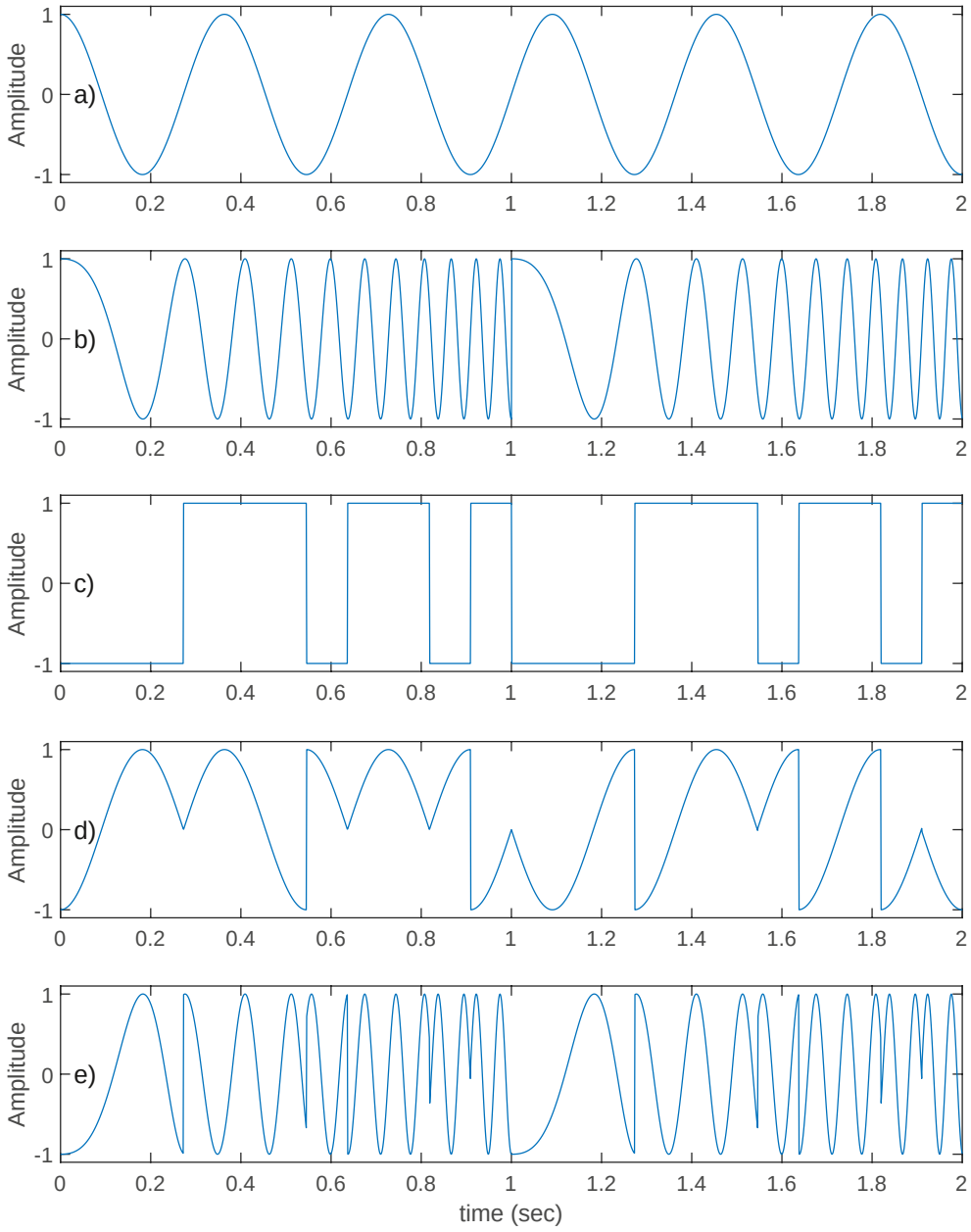

FIGURE 1 Illustration of the real part of typical radar waveforms. (a) Continuous waveform signal. (b) Frequency-modulated continuous waveform signal. (c) Binary phase code (baseband binary phase shift keying signal). (d) Phase-modulated continuous waveform signal. (e) Phase-coded frequency-modulated continuous waveform signal

the phase corresponding to the nth bit of the L_a bit sequence. Then, to realise a binary phase shift keying (BPSK), which is the current technology in automotive radars [27], the phase term spans $\phi_n \in \{0, \pi\}$.

The received signal reflected from the target can be written as:

$$x_{r_{target}}(t) = \sqrt{P_{target}} \sum_{n=1}^{L_a} e^{j\phi_n} \text{rect}\left(\frac{t-\tau-(n-1/2)T_a}{T_a}\right) \times \exp\left(j2\pi\left(f_c(t-\tau)+\frac{1}{2}k(t-\tau)^2\right)\right), \quad (6)$$

where τ is the time delay between the victim radar and the target. The constant phase term due to the scattering coefficient from target is omitted in the derivation for simplicity. If we assume the received interference is also PC-FMCW, it can be written as:

$$x_{r_{int}}(t) = \sqrt{P_{int}} \sum_{n=1}^{L_b} e^{j\phi_n} \text{rect}\left(\frac{t-\tau_{int}-(n-1/2)T_b}{T_b}\right) \times \exp\left(j2\pi\left(f_{c_{int}}(t-\tau_{int})+\frac{1}{2}k_{int}(t-\tau_{int})^2\right)\right), \quad (7)$$

where τ_{int} is the time delay between the victim and interfering radars, $f_{c_{int}}$ is the carrier frequency, k_{int} is the slope, L_b is the number of chips within one sweep, $T_b = T_{int}/L_b$ is the chip duration and T_{int} is the sweep duration of the interfering radar, respectively. Moreover, P_{target} and P_{int} are the received powers of the target echo and the interference, respectively, and can be obtained as:

$$P_{target} = \frac{P_t G_t G_r \lambda^2 \sigma}{(4\pi)^3 R^4_{target}}, \text{ and } P_{int} = \frac{P_{t_{int}} G_{t_{int}} G_r \lambda^2_{int}}{(4\pi)^2 R^2_{int}}.$$

Here λ is the wavelength, G_t is the gain of the transmitting antenna, and G_r is the gain of the receiving antenna for the victim radar. Similarly, λ_{int} is the wavelength, $P_{t_{int}}$ is the transmitting power, and $G_{t_{int}}$ is the gain of the transmitting antenna for the interferer radar. The σ is the radar cross-section of the target, and R_{target} and R_{int} are the range of target and interferer radar, respectively. It should be noted that the power of interference is inversely proportional to the interference range, shown as $P_{int} \propto R^{-2}_{int}$, while the target echo is inversely proportional with target range, described as $P_{target} \propto R^{-4}_{target}$. This may lead to the reception of a strong interferer signal that can mask the weak target echos.

The received signal in the victim radar, which includes the interfering signal, can be represented as:

$$x_r(t) = x_{r_{target}}(t) + x_{r_{int}}(t). \tag{8}$$

In this study we use complex signals representation for ease of mathematical manipulations and we assume a complex mixer is used. Note that the real signal representation should be used for a real heterodyne receiver. The received signal is mixed with the complex conjugate of uncoded transmitting signal for the dechirping process. The (complex) mixer output can be written as:

$$\begin{aligned} x_m(t) &= x_{r_{target}}(t) x_{t_{uc}}(t)^* + x_{r_{int}}(t) x_{t_{uc}}(t)^* \\ &= x_{m_{target}}(t) + x_{m_{int}}(t), \end{aligned} \tag{9}$$

where the uncoded transmitting signal is equal to the FMCW [25] and can be represented as $x_{t_{uc}}(t) = x_{t_{FMCW}}(t)$. In addition, $*$ denotes the complex conjugate. The mixer output consists of two components, namely the target and the interference. Explicitly, the target component can be obtained as:

$$\begin{aligned} x_{m_{target}}(t) &= x_{r_{target}}(t) x_{t_{uc}}(t)^* \\ &= \sqrt{P_{m_{target}}} \sum_{n=1}^{L_a} e^{j\phi_n} \text{rect}\left(\frac{t - \tau - (n - 1/2)T_a}{T_a}\right) \\ &\quad \times \exp\left(-j2\pi\left(f_c\tau + k\tau t - \frac{1}{2}k\tau^2\right)\right), \end{aligned} \tag{10}$$

where $P_{m_{target}} = P_{target} P_t$. Instantaneous spectrum can be used to determine the range of the target or the frequency of the interfering signal. If the instantaneous spectrum has a continuous part, it indicates either phase jumps caused by phase coding of the signal as the instantaneous frequency is a derivative of the signal phase [13] or reception of the spread-spectrum interfering signal. Thus, the instantaneous frequency spectrum provides additional information about the signal features, which cannot be observed in time-domain representation and it can be used to characterise the signal waveform. The phase of the mixer output related to the target echo is obtained as:

$$\phi_{m_{target}}(t) = -2\pi\left(f_c\tau + k\tau t - \frac{1}{2}k\tau^2\right) + \phi_{tar_{code}}(t), \tag{11}$$

where

$$\phi_{tar_{code}}(t) = \sum_{n=1}^{L_a} \phi_n \text{rect}\left(\frac{t - \tau - (n - 1/2)T_a}{T_a}\right) \tag{12}$$

Then, the instantaneous frequency of the mixer output of the target echo can be written as (see Appendix for details):

$$\begin{aligned} f_{i_{target}}(t) &= \frac{1}{2\pi}\frac{d}{dt}\phi_{m_{target}}(t) \\ &= \frac{1}{2\pi}(-2\pi(k\tau)) + \frac{1}{2\pi}\frac{d}{dt}\phi_{tar_{code}}(t) \\ &= -k\tau + \frac{1}{2\pi}\sum_{n=1}^{L_a}(\phi_{n+1} - \phi_n)\delta(t - \tau - nT_a). \end{aligned} \tag{13}$$

Similarly, the interference part is equal to:

$$\begin{aligned} x_{m_{int}}(t) &= x_{r_{int}}(t) x_{t_{uc}}(t)^* \\ &= \sqrt{P_{m_{int}}} \sum_{n=1}^{L_b} e^{j\phi_n} \text{rect}\left(\frac{t - \tau_{int} - (n - 1/2)T_b}{T_b}\right) \\ &\quad \times \exp\big(-j2\pi\big(t(f_c - f_{c_{int}} + k_{int}\tau_{int}) + f_{c_{int}}\tau_{int} \\ &\quad + t^2\left(\frac{1}{2}k - \frac{1}{2}k_{int}\right) - \frac{1}{2}k_{int}\tau^2_{int}\big)\big), \end{aligned} \tag{14}$$

where $P_{m_{int}} = P_{int} P_t$. The phase of the mixer output related to the received interference is obtained as:

$$\begin{aligned} \phi_{m_{int}}(t) &= -2\pi\big(t(f_c - f_{c_{int}} + k_{int}\tau_{int}) + f_{c_{int}}\tau_{int} \\ &\quad + t^2\left(\frac{1}{2}k - \frac{1}{2}k_{int}\right) - \frac{1}{2}k_{int}\tau^2_{int}\big) \\ &\quad + \phi_{int_{code}}(t), \end{aligned} \tag{15}$$

where

$$\phi_{int_{code}}(t) = \sum_{n=1}^{L_b} \phi_n \text{rect}\left(\frac{t - \tau_{int} - (n-1/2)T_b}{T_b}\right) \quad (16)$$

Subsequently, the instantaneous frequency of the mixer output of received interference can be obtained as (see Appendix for details):

$$\begin{aligned} f_{i_{int}}(t) &= \frac{1}{2\pi}\frac{d}{dt}\phi_{m_{int}}(t) \\ &= t(k_{int} - k) + (f_{c_{int}} - f_c - k_{int}\tau_{int}) \\ &\quad + \frac{1}{2\pi}\frac{d}{dt}\phi_{int_{code}}(t) \\ &= t(k_{int} - k) + (f_{c_{int}} - f_c - k_{int}\tau_{int}) \\ &\quad + \frac{1}{2\pi}\sum_{n=1}^{L_b}(\phi_{n+1} - \phi_n)\delta(t - \tau_{int} - nT_b). \end{aligned} \quad (17)$$

Finally, the mixer output in the victim radar can be recast as:

$$\begin{aligned} x_m(t) = &\sqrt{P_{m_{target}}}\exp\left(j\phi_{m_{target}}(t)\right) \\ &+ \sqrt{P_{m_{int}}}\exp\left(j\phi_{m_{int}}(t)\right), \end{aligned} \quad (18)$$

and the instantaneous frequency of the mixer output equals to the derivative of the phase terms in Equation (18) and it consists of $f_{i_{target}}(t)$ and $f_{i_{int}}(t)$, shown as:

$$f_{i_m}(t) \supseteq \{f_{i_{target}}(t), f_{i_{int}}(t)\}. \quad (19)$$

where $B \supseteq A$ denotes 'B is a superset of A'.

It is important to note that the time-domain representation of the mixer output alone does not demonstrate all features of the interference. The interference appearance at the beat frequency is related to the waveform parameters and can be observed in time-frequency analysis (instantaneous frequency signature in spectrogram). Thus, we analysed the instantaneous frequency of the mixer output and mathematically modelled the signals at the victim radar. The instantaneous frequency of the mixer output on the victim radar depends on the difference between chirp slopes for a given time, described as $t(k_{int} - k)$, plus the difference between carrier frequencies $(f_{c_{int}} - f_c)$ minus the corresponding beat frequencies for both the target echo and the interference, illustrated as $-k_{int}\tau_{int} - k\tau$, plus a summation of Dirac deltas due to the immediate phase changes.

Here, Equations (18) and (19) represent the generalised radar-to-radar interference equation and its instantaneous frequency, respectively. The target and the interference response on the victim radar for different waveforms can be obtained using the proposed generalised radar-to-radar interference equation by setting the variables (L_a, k, L_b and k_{int}) as defined in Table 1.

TABLE 1 Different waveform scenarios

Victim	Interference	L_a	k	L_b	k_{int}
CW	CW	$= 0$	$= 0$	$= 0$	$= 0$
CW	FMCW	$= 0$	$= 0$	$= 0$	$\neq 0$
CW	PMCW	$= 0$	$= 0$	$\neq 0$	$= 0$
CW	PC-FMCW	$= 0$	$= 0$	$\neq 0$	$\neq 0$
FMCW	CW	$= 0$	$\neq 0$	$= 0$	$= 0$
FMCW	FMCW	$= 0$	$\neq 0$	$= 0$	$\neq 0$
FMCW	PMCW	$= 0$	$\neq 0$	$\neq 0$	$= 0$
FMCW	PC-FMCW	$= 0$	$\neq 0$	$\neq 0$	$\neq 0$
PMCW	CW	$\neq 0$	$= 0$	$= 0$	$= 0$
PMCW	FMCW	$\neq 0$	$= 0$	$= 0$	$\neq 0$
PMCW	PMCW	$\neq 0$	$= 0$	$\neq 0$	$= 0$
PMCW	PC-FMCW	$\neq 0$	$= 0$	$\neq 0$	$\neq 0$
PC-FMCW	CW	$\neq 0$	$\neq 0$	$= 0$	$= 0$
PC-FMCW	FMCW	$\neq 0$	$\neq 0$	$= 0$	$\neq 0$
PC-FMCW	PMCW	$\neq 0$	$\neq 0$	$\neq 0$	$= 0$
PC-FMCW	PC-FMCW	$\neq 0$	$\neq 0$	$\neq 0$	$\neq 0$

Abbreviations: CW, continuous waveform; FMCW, frequency-modulated continuous waveform; PC-FMCW, phase-coded frequency-modulated continuous waveform; and PMCW, phase-modulated continuous waveform.

3 | CONVERGENCE OF THE GENERALISED INTERFERENCE EQUATION

In this section, the convergence of the generalised radar-to-radar interference equation is explained. Various waveforms are used in automotive radar applications. Different kinds of interference types, therefore, can be observed under various radar setups. The generalised radar-to-radar interference equation covers all the scenarios given in Table 1 and can be applied to particular cases. Consequently, the proposed equation can be used to model and simulate interference on the victim radar. To illustrate the effectiveness of the generalised radar-to-radar interference equation, we consider the following most common scenarios for automotive radars.

3.1 | FMCW radar versus FMCW interferer

Assume both the victim and interferer radars use FMCW. As most automotive radars use FMCW, this scenario is very common on the road. Thus, various interference mitigation methods have been studied for this scenario, such as [28–30]. Following Table 1, set $L_a = 0$, $k \neq 0$, $L_b = 0$ and $k_{int} \neq 0$ in Equations (18) and (19) to achieve the FMCW radar versus FMCW interferer case. The mixer output on the victim radar becomes:

$$x_m(t) = \sqrt{P_{m_{target}}}\exp\Big(-j2\pi\Big(f_c\tau + k\tau t - \frac{1}{2}k\tau^2\Big)\Big) + \sqrt{P_{m_{int}}}\exp\Big(-j2\pi\Big(f_{c_{int}}\tau_{int} + t(f_c - f_{c_{int}} + k_{int}\tau_{int}) + t^2\Big(\frac{1}{2}k - \frac{1}{2}k_{int}\Big) - \frac{1}{2}k_{int}\tau_{int}^2\Big)\Big), \quad (20)$$

and its instantaneous frequency consists of:

$$f_{i_m}(t) \supseteq \{f_{i_{target}}(t), f_{i_{int}}(t)\}, \quad (21a)$$

$$f_{i_{target}}(t) = -k\tau, \quad (21b)$$

$$f_{i_{int}}(t) = t(k_{int} - k) + (f_{c_{int}} - f_c) - k_{int}\tau_{int}. \quad (21c)$$

Note that the results are the same as those given in [31–33].

In Figure 2, the instantaneous frequency of the mixer output for the FMCW victim radar is simulated by using the derived equation in cases of FMCW versus FMCW. We chose interference parameters with different chirp slopes, carrier frequencies and delays, such that the captured interference leads to the 'V-shape'. Here the $(f_{c_{int}} - f_c)$ and the $-k_{int}\tau_{int}$ terms determine the starting point of the captured interference, while the $t(k_{int} - k)$ term controls the slope of the 'V-shape' and the wider or narrower interference shape can be observed depending on this term. In addition, the $-k\tau$ term is the beat signal induced by the target; it is illustrated with the blue colour in Figure 2.

3.2 | FMCW radar versus CW interferer

We can realise this scenario by choosing $L_a = 0$, $k \neq 0$, $L_b = 0$ and $k_{int} = 0$ in Equations (18) and (19). The mixer output on the victim radar becomes:

$$x_m(t) = \sqrt{P_{m_{target}}}\exp\Big(-j2\pi\Big(f_c\tau + k\tau t - \frac{1}{2}k\tau^2\Big)\Big) + \sqrt{P_{m_{int}}}\exp\Big(-j2\pi\Big(f_{c_{int}}\tau_{int} + t(f_c - f_{c_{int}}) + \frac{1}{2}kt^2\Big)\Big), \quad (22)$$

and its instantaneous frequency consists of:

$$f_{i_m}(t) \supseteq \{f_{i_{target}}(t), f_{i_{int}}(t)\}, \quad (23a)$$

$$f_{i_{target}}(t) = -k\tau, \quad (23b)$$

$$f_{i_{int}}(t) = t(-k) + (f_{c_{int}} - f_c). \quad (23c)$$

3.3 | PMCW radar versus PMCW interferer

The phase-modulated continuous waveform is usually used for communication purposes [32]. In addition, it may provide possible improvement against interference [34, 35]. Therefore, it has been used in automotive radars in particular cases. It is possible to investigate such a scenario by allowing $L_a \neq 0$, $k = 0$, $L_b \neq 0$ and $k_{int} = 0$ [Equations (18) and (19)]. The mixer output on the victim radar becomes:

$$x_m(t) = \sqrt{P_{m_{target}}}\exp(-j2\pi(f_c\tau) + \phi_{tar_{code}}(t)) + \sqrt{P_{m_{int}}}\exp\Big(-j2\pi\Big(f_{c_{int}}\tau_{int} + t(f_c - f_{c_{int}})\Big) + \phi_{int_{code}}(t)\Big), \quad (24)$$

and its instantaneous frequency consists of:

$$f_{i_m}(t) \supseteq \{f_{i_{target}}(t), f_{i_{int}}(t)\}, \quad (25a)$$

$$f_{i_{target}}(t) = \frac{1}{2\pi}\sum_{n=1}^{L_a}(\phi_{n+1} - \phi_n)\delta(t - \tau - nT_a), \quad (25b)$$

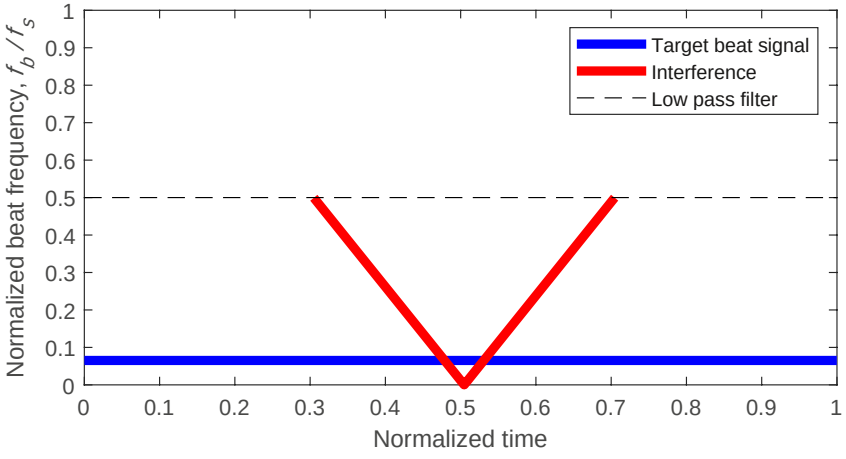

FIGURE 2 Simulation of FMCW versus FMCW. Instantaneous frequency of the mixer output for the FMCW victim radar is simulated by using the derived equation

$$f_{i_{int}}(t) = (f_{c_{int}} - f_c) + \frac{1}{2\pi}\sum_{n=1}^{L_b}(\phi_{n+1} - \phi_n)\delta(t - \tau_{int} - nT_b). \quad (25c)$$

3.4 | FMCW radar versus PMCW interferer

The impacts of PMCW interference on FMCW radar are studied in [36]. In addition to that study, we can analyse the interference features for this specific scenario by setting $L_a = 0$, $k \neq 0$, $L_b \neq 0$ and $k_{int} = 0$ [Equations (18) and (19)]. The mixer output on the victim radar becomes:

$$\begin{aligned} x_m(t) &= \sqrt{P_{m_{target}}}\exp\big(-j2\pi\big(f_c\tau + k\tau t - \frac{1}{2}k\tau^2\big)\big) \\ &+ \sqrt{P_{m_{int}}}\exp\big(-j2\pi\big(f_{c_{int}}\tau_{int} \\ &+ t(f_c - f_{c_{int}}) + \frac{1}{2}kt^2\big) + \phi_{int_{code}}(t)\big), \end{aligned} \quad (26)$$

and its instantaneous frequency consists of:

$$f_{i_m}(t) \supseteq \{f_{i_{target}}(t), f_{i_{int}}(t)\}, \quad (27a)$$

$$f_{i_{target}}(t) = -k\tau, \quad (27b)$$

$$f_{i_{int}}(t) = t(-k) + (f_{c_{int}} - f_c) + \frac{1}{2\pi}\sum_{n=1}^{L_b}(\phi_{n+1} - \phi_n)\delta(t - \tau_{int} - nT_b). \quad (27c)$$

3.5 | PC-FMCW radar versus PC-FMCW interferer

The scenario in which PC-FMCW radar is interfered with by another PC-FMCW can be explored by choosing $L_a \neq 0$, $k \neq 0$, $L_b \neq 0$ and $k_{int} \neq 0$ [Equations (18) and (19)]. The mixer output on victim radar becomes:

$$\begin{aligned} x_m(t) &= \sqrt{P_{m_{target}}}\exp\big(-j2\pi\big(f_c\tau + k\tau t - \frac{1}{2}k\tau^2\big) \\ &+ \phi_{tar_{code}}(t)\big) \\ &+ \sqrt{P_{m_{int}}}\exp\big(-j2\pi\big(f_{c_{int}}\tau_{int} \\ &+ t(f_c - f_{c_{int}} + k_{int}\tau_{int}) \\ &+ t^2\big(\frac{1}{2}k - \frac{1}{2}k_{int}\big) - \frac{1}{2}k_{int}\tau_{int}^2\big) + \phi_{int_{code}}(t)\big), \end{aligned} \quad (28)$$

and its instantaneous frequency consists of:

$$f_{i_m}(t) \supseteq \{f_{i_{target}}(t), f_{i_{int}}(t)\}, \quad (29a)$$

$$f_{i_{target}}(t) = -k\tau + \frac{1}{2\pi}\sum_{n=1}^{L_a}(\phi_{n+1} - \phi_n)\delta(t - \tau - nT_a), \quad (29b)$$

$$f_{i_{int}}(t) = t(k_{int} - k) + (f_{c_{int}} - f_c) - k_{int}\tau_{int} + \frac{1}{2\pi}\sum_{n=1}^{L_b}(\phi_{n+1} - \phi_n)\delta(t - \tau_{int} - nT_b). \quad (29c)$$

3.6 | FMCW radar versus PC-FMCW interferer

We can observe this scenario by using the generalised radar-to-radar interference equation, letting $L_a = 0$, $k \neq 0$, $L_b \neq 0$ and $k_{int} \neq 0$ [Equations (18) and (19)]. The mixer output on the victim radar becomes:

$$\begin{aligned} x_m(t) &= \sqrt{P_{m_{target}}}\exp\big(-j2\pi\big(f_c\tau + k\tau t - \frac{1}{2}k\tau^2\big)\big) \\ &+ \sqrt{P_{m_{int}}}\exp\big(-j2\pi\big(f_{c_{int}}\tau_{int} \\ &+ t(f_c - f_{c_{int}} + k_{int}\tau_{int}) \\ &+ t^2\big(\frac{1}{2}k - \frac{1}{2}k_{int}\big) - \frac{1}{2}k_{int}\tau_{int}^2\big) + \phi_{int_{code}}(t)\big), \end{aligned} \quad (30)$$

and its instantaneous frequency consists of:

$$f_{i_m}(t) \supseteq \{f_{i_{target}}(t), f_{i_{int}}(t)\}, \quad (31a)$$

$$f_{i_{target}}(t) = -k\tau, \quad (31b)$$

$$f_{i_{int}}(t) = t(k_{int} - k) + (f_{c_{int}} - f_c) - k_{int}\tau_{int} + \frac{1}{2\pi}\sum_{n=1}^{L_b}(\phi_{n+1} - \phi_n)\delta(t - \tau_{int} - nT_b). \quad (31c)$$

In Figure 3 the instantaneous frequency of the mixer output for the FMCW victim radar is simulated by using the derived equation in the case of FMCW versus PC-FMCW. For ease of comparison, we used the same interference parameters that we selected in the FMCW versus FMCW case. As a result, the $t(k_{int} - k)$ term causes the 'V-shape' for the captured interference, with the starting point being controlled by the $(f_{c_{int}} - f_c)$ and $-k_{int}\tau_{int}$ terms. In addition to the 'V-shape', we observe the Dirac deltas on the instantaneous frequency of the victim radar due to the phase coding of the interference. The phase sequence changes from 0 to π and from π to 0 for the PC-FMCW interferer radar, as shown in Figure 3.

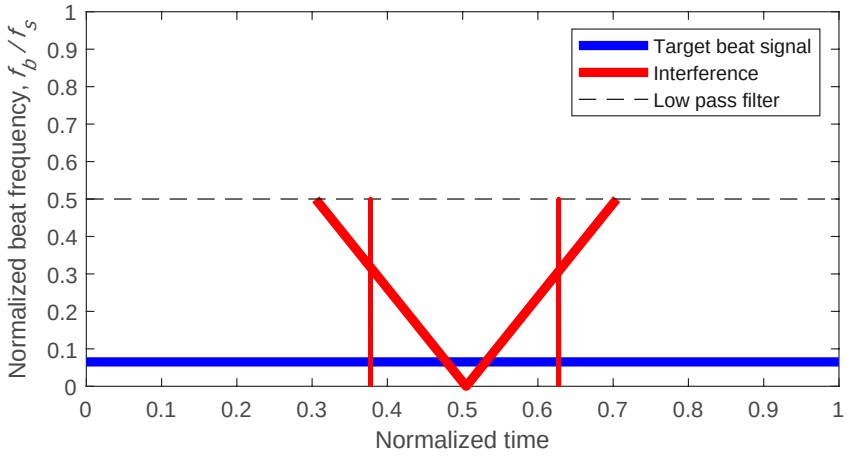

FIGURE 3 Simulation of FMCW versus PC-FMCW. Instantaneous frequency of the mixer output for the FMCW victim radar is simulated by using the derived equation

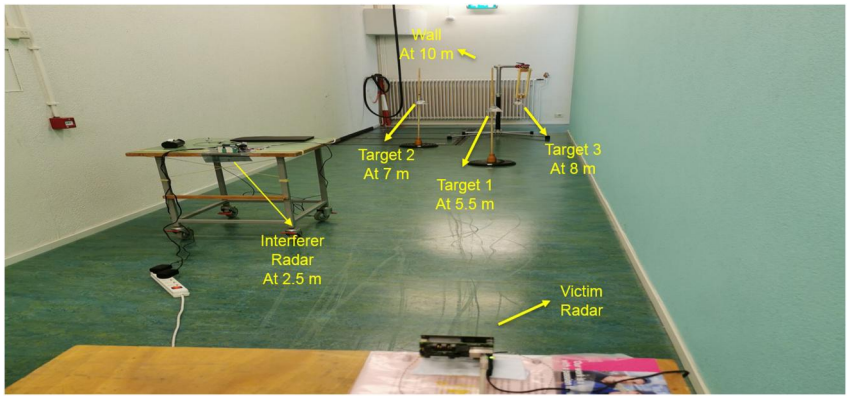

FIGURE 4 Experimental setup

TABLE 2 System parameters

		Victim	Interference
Sweep duration	T	102.4 μs	102.4 μs
Bandwidth	B	1.155 GHz	1.2 GHz
Carrier frequency	f_c	78.915 GHz	78.98 GHz
Sampling frequency	f_s	10 MHz	10 MHz
Number of coding chips	L_c	4	4

4 | EXPERIMENTS AND UTILISATION

This section provides the experimental verification of the proposed generalised radar-to-radar interference equation and discusses its utilisation.

4.1 | Experimental verification

In this section we demonstrate the experimental results. Using commercially available off-the-shelf (COTS) automotive radar sensors, multiple NXP automotive radar chipsets and their microcontrollers (TEF810X and S32R274) were programed for phase coding as described in [27] and were synchronised to simulate the worst case scenario as described in [24]. The experimental setup included victim radar, interfering radar, and controlled stationary and moving targets as shown in Figure 4. In the experiments we focussed on investigating the following four scenarios: FMCW versus FMCW, PC-FMCW versus FMCW, FMCW versus PC-FMCW and PC-FMCW versus PC-FMCW. We used BPSK code sequence with 4 chips to be able to observe the phase changes in our outputs clearly. The transmitted code for the PC-FMCW radars was set to [1, −1, −1, and 1], which corresponds to a phase change between 0 and π according to the code sequence. We used a time-frequency analysis, namely a spectrogram, to investigate the mixer output signals of the victim radar. To mimic a worst-case scenario we selected the system parameters such that interfering radar signals passed through the LPF of the victim radar and were captured by the victim radar's analogue-to-digital converter (ADC) within the observation time. These system parameters for the experiments are given in Table 2.

Note that the effects of the filters are not shown Equations (19), as each system has its own filter response. In general, the impact of a filter on the instantaneous frequency of the code term can be written as:

$$g(t) = f_{i_{code}}(t) \otimes h(t), \tag{32}$$

where $\otimes$ represents the convolution and $f_{i_{code}}(t)$ is the instantaneous frequency of the code. For mathematical

representation, if we choose $h(t)$ as an ideal brick-wall filter, the equation becomes:

$$g(t) = \frac{f_{cut}}{2} \sum_{n=1}^{L_c} (\phi_{n+1} - \phi_n) \text{sinc}\left(\frac{f}{f_{cut}}\right), \quad (33)$$

where f_{cut} is the cut-off frequency of the low-pass filter and L_c is the number of chips within one sweep for the victim or interferer radar. In this experiment the convolution of Dirac deltas (due to the BPSK code) and the cascaded filter response created a transient region (short burst of oscillation) in one system when there was a sudden phase change.

In the first experiment we used FMCW for both victim and interfering radars to verify Equation (21). In the second experiment we changed the signal transmitted by the victim radar to PC-FMCW and investigated the FMCW interference on the PC-FMCW radar. In the third experiment we used FMCW as a victim radar and examined the effects of PC-FMCW as an interference on the FMCW radar. In the fourth and final experiment we used PC-FMCW for both victim radar and interfering radars to verify Equation (29). Note that the spectrogram parameters have been adjusted to emphasise the interference. The results are discussed in the following subsections.

4.1.1 | Scenario 1 (FMCW victim radar vs. FMCW interferer)

The mixer output is shown in Figure 5, where the beat frequencies and the captured interfering signal are observed. According to Equation (21) we expected the time-dependent term $t(k_{int} - k)$ plus the difference between carrier frequencies $(f_{c_{int}} - f_c)$ minus the corresponding beat frequencies for both target echo and interference, as $-k_{int}\tau_{int} - k\tau$. As demonstrated in Figure 5, the target and interference returns induced the beat frequencies (shown in the white rectangle), while the interfering signal created a 'V-shaped' signature (shown in the black rectangle) in the instantaneous frequency of the FMCW victim radar. The time-dependent term $t(k_{int} - k)$ resulted in a 'V-shape' for the chosen system parameters.

4.1.2 | Scenario 2 (PC-FMCW radar vs. FMCW interferer)

The immediate phase changes caused the transient region as discussed Equations (32). Therefore, we also expected to see a transient region due to immediate phase changes used on the victim radar's PC-FMCW waveform as $(\phi_{n+1} - \phi_n)\delta(t - \tau - nT_a) \otimes h(t)$. These transient regions are observable in Figure 6 when the phase changes from 0 to π and from π to 0. In addition, the target and FMCW interference induced beat frequencies and 'V-shaped' interference, respectively.

4.1.3 | Scenario 3 (FMCW radar vs. PC-FMCW interferer)

In this case we expected to obtain a transient region due to immediate phase changes applied to the interferer PC-FMCW radar. This transient region equals to $(\phi_{n+1} - \phi_n)\delta(t - \tau_{int} - nT_b) \otimes h(t)$, according to Equations (31) and (32). When the phase changed, the interferer PC-FMCW radar did cause a weak transient region along with 'V-shaped' interference on the FMCW victim radar, as illustrated in Figure 7.

4.1.4 | Scenario 4 (PC-FMCW radar vs. PC-FMCW interferer)

In this final scenario we expected to obtain beat signals $-k_{int}\tau_{int} - k\tau$ and the time-dependent term $t(k_{int} - k)$

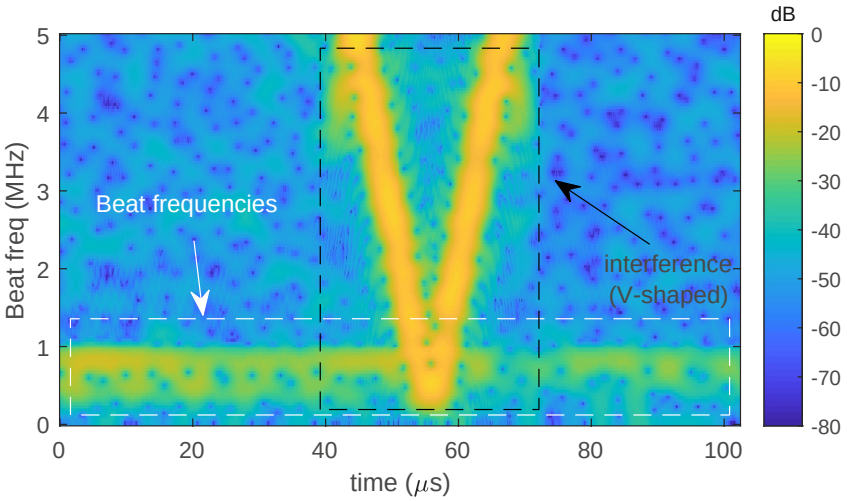

FIGURE 5 FMCW versus FMCW. Instantaneous frequency of the mixer output for FMCW victim radar. There are no transient regions or abrupt phase changes due to coding as a frequency column in the spectrogram. Only 'V-shaped' interference is observable

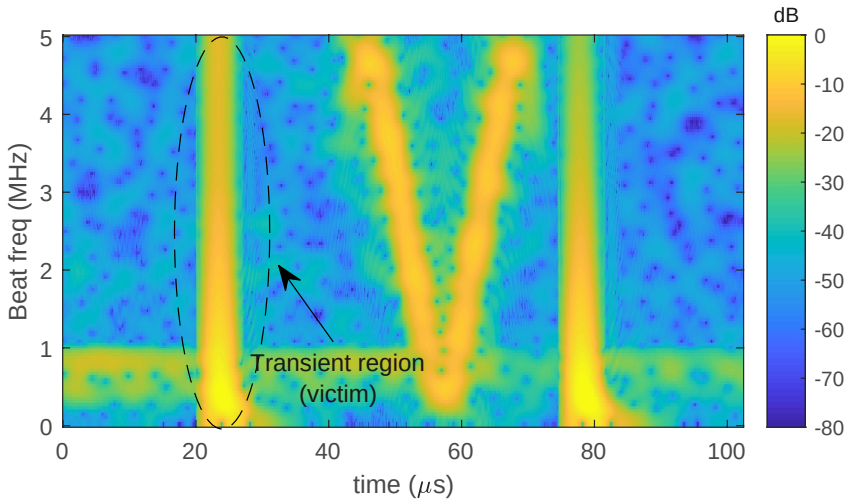

FIGURE 6 PC-FMCW versus FMCW. Instantaneous frequency of the mixer output for PC-FMCW victim radar. The abrupt phase changes due to coding are observable as a frequency column in the spectrogram. In this particular pulse the code sequence is [0, π, π, 0]

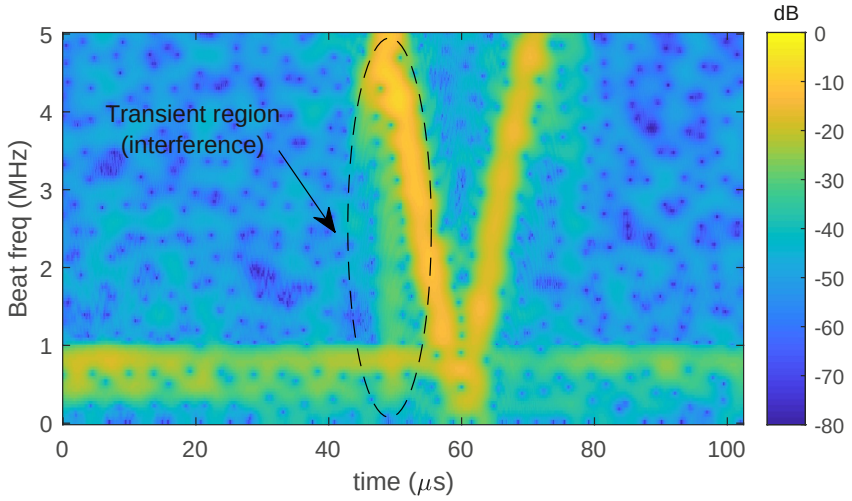

FIGURE 7 FMCW versus PC-FMCW. Instantaneous frequency of the mixer output for FMCW victim radar. The abrupt phase changes due to coding are observable as a frequency column in the spectrogram. In this particular pulse the code sequence is [0, π, π, 0]

due to FMCW part of the interference. In addition to these terms, both the victim and the interferer PC-FMCW radars caused the following transient regions: $(\phi_{n+1} - \phi_n)\delta(t - \tau - nT_a) \otimes h(t)$ and $(\phi_{n+1} - \phi_n)\delta(t - \tau_{int} - nT_b) \otimes h(t)$, according to Equations (29) and (32). As demonstrated in Figure 8, the corresponding beat frequencies and the 'V-shaped' interference were obtained on the spectrogram. Furthermore, the victim PC-FMCW radar created the transient regions (shown in the black circle), and the interfering PC-FMCW radar produced the weak transient region (shown in the white circle) during the phase changes.

4.2 | Utilisation

The proposed equation can model most of the common types of automotive radar interference at the beat (intermediate) frequency. Moreover, the equation can help to determine analytically the slope of the 'V-shape' as a function of system parameters of interfering radar. Hence, the equation can be used to simulate different interference scenarios accurately and support the analysis of impact of various interference types on target detection. In addition, the instantaneous beat frequency of the victim radar for the selected waveforms can be modelled by using the proposed equation. These interference models obtained by the proposed equation can be utilised to create a data set for the interference classification and they might be used to train a neural network (NN) [37]. The application of the proposed interference equation to those fields is left as future research topic.

5 | DISCUSSION

5.1 | Different phase modulation scheme

This study has focussed on BPSK, as it is commonly used for COTS radar systems such as PMCW [15] and PC-FMCW [25]. Therefore, the phase of the code term has discrete values (0 or π) during chip duration, as shown Equation (5). However, different phase modulation schemes can have phase values that

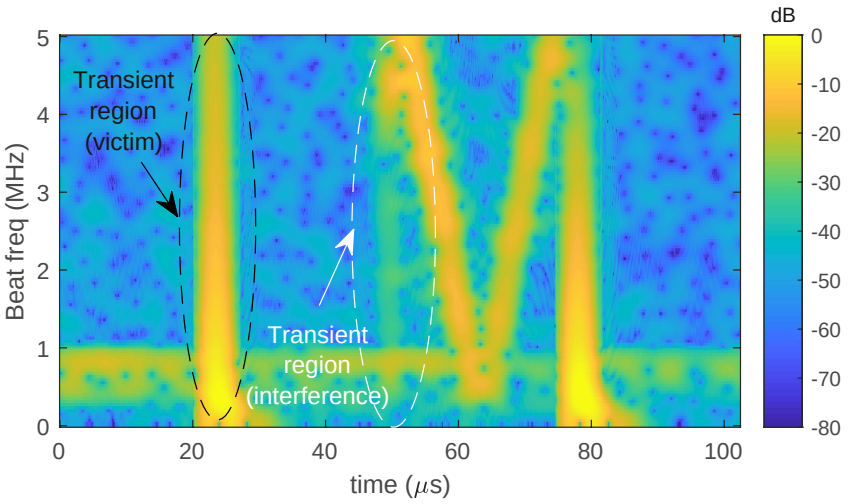

FIGURE 8 PC-FMCW versus PC-FMCW. Instantaneous frequency of the mixer output for PC-FMCW victim radar. The abrupt phase changes due to coding are observable as a frequency column in the spectrogram. In this particular pulse the code sequence is [0, π, π, 0]

vary over time. To include such a case, we can generally rewrite the phase term of the code as:

$$c_t(t) = e^{j\phi(t)}. \tag{34}$$

If the transmitted phase code of the victim radar has a value that is a function of time, the (12) and (13) need to be updated as:

$$\phi_{tar_{code}}(t) = \phi(t), \tag{35}$$

and

$$f_{i_{target}}(t) = -k\tau + \frac{1}{2\pi}\frac{d}{dt}\phi(t), \tag{36}$$

respectively. Similarly, Equations (16) and (17) should be updated accordingly for the interferer signal in cases where the phase value varies over time.

5.2 | Multiple interference

In this study we have investigated the fundamental problem of interference for different waveforms in the context of a single-input single-output (SISO) system. Multiple transmitters within the same transceiver (such as a MIMO system), other radars present on the same car and in the environment can cause multiple interference. When multiple interferers overlap in frequency and/or time, their combined impact can be computed as the superposition of all interferers, while the impact of a single interferer can be obtained using the proposed equation, such that the mixer output on the victim radar becomes:

$$\begin{aligned} x_m(t) &= \sum_{r=1}^{R} x_{m_{target,r}}(t) + \sum_{p=1}^{P} x_{m_{int,p}}(t) \\ &= \sum_{r=1}^{R}\Bigg\{\sqrt{P_{m_{target,r}}}\exp\Big(-j2\pi\Big(f_c\tau_r + k\tau_r t - \frac{1}{2}k{\tau_r}^2\Big) \\ &\quad + \phi_{tar_{code}}(t)\Big)\Bigg\} \\ &\quad + \sum_{p=1}^{P}\Bigg\{\sqrt{P_{m_{int,p}}}\exp\Big(-j2\pi\Big(f_{c_{int,p}}\tau_{int,p} \\ &\quad + t(f_c - f_{c_{int,p}} + k_{int,p}\tau_{int,p}) + t^2\Big(\frac{1}{2}k - \frac{1}{2}k_{int,p}\Big) \\ &\quad - \frac{1}{2}k_{int,p}\tau_{int,p}^2\Big) + \phi_{int_{code,p}}(t)\Big)\Bigg\}, \end{aligned} \tag{37}$$

and the instantaneous frequency of the mixer output consists of:

$$\begin{aligned} f_{i_m}(t) \supseteq \Big\{&f_{i_{target,1}}(t), \ldots, f_{i_{target,R}}(t), \\ &\Big\{f_{i_{int,1}}(t), \ldots, f_{i_{int,p}}(t)\Big\}, \end{aligned} \tag{38}$$

where $x_{m_{target,r}}(t)$ is the mixer output and $f_{i_{target,r}}$ is the instantaneous frequency induced by the rth target ($0 < r < R$). Similarly, the $x_{m_{int,p}}(t)$ is the mixer output and $f_{i_{int,p}}$ is the instantaneous frequency induced by the pth interferer ($0 < p < P$). In Figure 9 the multiple interference scenarios for FMCW versus FMCW is simulated. There we assume that each captured interference has a different chirp slope and carrier frequency. We also consider a second target with a different range and demonstrate its beat frequency on the victim radar. Similarly, the impact of the distributed targets can be calculated as the linear superposition of the waveforms transmitted by the same radar.

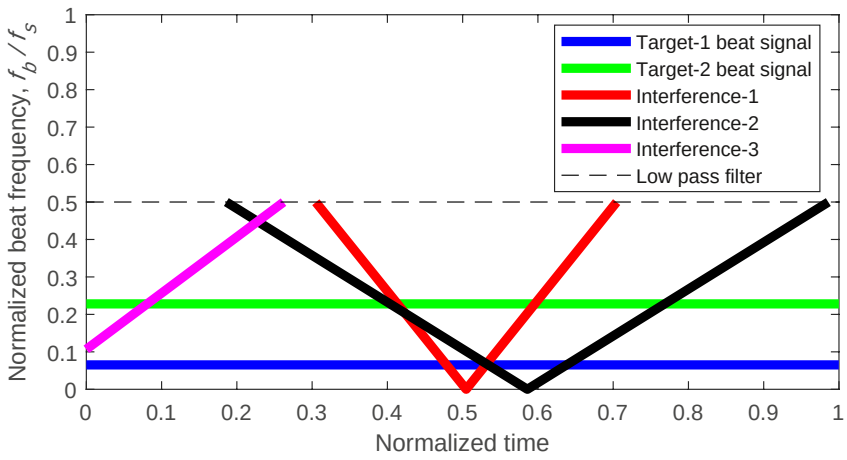

FIGURE 9 Simulation of multiple interference. Instantaneous frequency of the mixer output on the FMCW victim radar for the multiple interference scenario is simulated by using the derived equation

For the MIMO system, there are three different kinds of MIMO transmission realisations: time division, frequency division and code division. Without losing generality, it is possible to extend our derivation and experimental evaluation to different MIMO systems. Since the analysis and experimental verification still need to be done for all 3^2 MIMO cases with 4^2 waveforms (combinations of victim and interference), these have not been included in this study.

6 | CONCLUSION

In this study we have studied the automotive radar interference and extended the radar-to-radar interference analysis for various types of continuous waveforms. We introduced a generalised radar-to-radar interference equation, which can be applied to different specific cases described in the literature. The derived generalised equation can be directly applied in cases of multiple interferers and multiple targets, as shown in the study. By using the proposed equation, it is possible to simulate various interference scenarios fast and accurately. Furthermore, the introduced equation describes the instantaneous beat frequency of the victim radar for different waveforms to examine the features of the interference. This knowledge can be exploited to identify the received interference type. Therefore, the proposed equation can assist in analysing the impacts of different interference types on target detection in automotive radar applications. In addition, the proposed equation can be used to create a data set for the interference classification.

The mutual interference analysis of different radar waveform types and the correctness of the derived equation was verified by experiments. Moreover, both the mathematical analysis of PC-FMCW interference and experimental verification of such a system in real-time automotive radar were demonstrated for the first time by using commercially available off-the-shelf automotive radar transceivers. Although this research focussed on the application in an automotive context, it can be used in other radar fields as well.

ACKNOWLEDGEMENTS

As part of the TU Delft Industry Partnership Program (TIPP), this research is funded by NXP Semiconductors N.V. and Holland High Tech Systems and Materials (TKI-HTSM/18.0136) under the project 'Coded Radar for Interference Suppression in Super-Dense Environments' (CRUISE). The authors would like to thank Nikita Petrov for his helpful suggestions and Simone Orru for his support during the experiments. Finally, the authors would like to thank the anonymous reviewers for their constructive comments that improved the quality of the study significantly.

CONFLICT OF INTEREST

We do not have any conflict of interest.

DATA AVAILABILITY STATEMENT

The data that support the findings of this study are available from the corresponding author upon reasonable request.

ORCID

Utku Kumbul https://orcid.org/0000-0002-1434-6008

REFERENCES

1. Kunert, M., et al.: Report on interference density increase by market penetration forecast. MOSARIM Consortium, CNTR, Technical Report. D16 (2010)
2. Brooker, G.M.: Mutual interference of millimeter-wave radar systems. IEEE Trans. Electromagn. Compat. 49(1), 170–181 (2007)
3. Bilik, I., et al.: The rise of radar for autonomous vehicles: signal processing solutions and future research directions. IEEE Signal Process. Mag. 36(5), 20–31 (2019)
4. Goppelt, M., Blöcher, H.L., Menzel, W.: Automotive radar investigation of mutual interference mechanisms. Adv. Radio Sci. 8, 55–60 (2010)
5. Schipper, T., et al.: Simulative prediction of the interference potential between radars in common road scenarios. IEEE Trans. Electromagn. Compat. 57(3), 322–328 (2015)

6. Sun, S., Petropulu, A.P., Poor, H.V.: Mimo radar for advanced driver-assistance systems and autonomous driving: advantages and challenges. IEEE Signal Process. Mag. 37(4), 98–117 (2020)
7. Bechter, J., Waldschmidt, C.: Automotive radar interference mitigation by reconstruction and cancellation of interference component. In: IEEE MTT-S International Conference on Microwaves for Intelligent Mobility (ICMIM), pp. 1–4 (2015)
8. Nozawa, T., et al.: An anti-collision automotive FMCW radar using time-domain interference detection and suppression. In: International Conference on Radar Systems, pp. 1–5 (2017)
9. Patole, S.M., et al.: Automotive radars: a review of signal processing techniques. IEEE Signal Process. Mag. 34(2), 22–35 (2017)
10. Aydogdu, C., et al.: Radar interference mitigation for automated driving: exploring proactive strategies. IEEE Signal Process. Mag. 37(4), 72–84 (2020)
11. Skolnik, M.I.: Introduction to Radar Systems, 2nd ed. McGraw-Hill, New York (1980)
12. Stove, A.G.: Linear FMCW radar techniques. IEE Proc. F Radar Signal Process. 139(5), 343–350 (1992)
13. Jankiraman, M.: FMCW Radar Design. Artech House, Massachusetts (2018)
14. Xu, Z., Shi, Q.: Interference mitigation for automotive radar using orthogonal noise waveforms. IEEE Geosci. Remote Sens. Lett. 15(1), 137–141 (2018)
15. Bourdoux, A., et al.: PMCW waveform and mimo technique for a 79 GHz CMOS automotive radar. In: IEEE Radar Conference (RadarConf), pp. 1–5 (2016)
16. Fan, P.Z., et al.: Class of binary sequences with zero correlation zone. Electron. Lett. 35(10), 777–779 (1999)
17. Richards, M.A.: Fundamentals of Radar Signal Processing. McGraw-Hill, New York (2005)
18. Blunt, S.D., et al.: Polyphase-coded fm (PCFM) radar waveforms, part I: implementation. IEEE Trans. Aerosp. Electron. Syst. 50(3), 2218–2229 (2014)
19. Blunt, S.D., Mokole, E.L.: Overview of radar waveform diversity. IEEE Aerosp. Electron. Syst. Mag. 31(11), 2–42 (2016)
20. García, E., et al.: Spreading sequences in active sensing: a review. Signal Process. 106, 88–105 (2015)
21. Reneau, J., Adhami, R.R.: Phase-coded IFMCW waveform analysis for short range measurement applications. In: IEEE Aerospace Conference, pp. 1–6 (2014)
22. McCormick, P.M., et al.: FMCW implementation of phase-attached radar-communications (PARC). In: IEEE Radar Conference (RadarConf), pp. 1–6 (2019)
23. Kumbul, U., et al.: Experimental investigation of phase coded FMCW for sensing and communications. In: 2021 15th European Conference on Antennas and Propagation (EuCAP), pp. 1–5 (2021)
24. Lampel, F., et al.: System level synchronization of phase-coded FMCW automotive radars for radcom. In: 2020 14th European Conference on Antennas and Propagation (EuCAP), pp. 1–5 (2020)
25. Uysal, F.: Phase-coded FMCW automotive radar: system design and interference mitigation. IEEE Trans. Veh. Technol. 69(1), 270–281 (2020)
26. Lampel, F., et al.: A performance enhancement technique for a joint FMCW radcom system. In: 2019 16th European Radar Conference (EuRAD), pp. 169–172 (2019)
27. Uysal, F., Orru, S.: Phase-coded FMCW automotive radar: application and challenges. In: IEEE International Radar Conference (RADAR), pp. 478–482 (2020)
28. Choi, J.H., et al.: Mutual interference suppression using clipping and weighted-envelope normalization for automotive FMCW radar systems. IEICE Trans. Commun. 99-B, 280–287 (2016)
29. Wagner, M., et al.: Threshold-free interference cancellation method for automotive FMCW radar systems. In: IEEE International Symposium on Circuits and Systems (ISCAS), pp. 1–4 (2018)
30. Umehira, M., et al.: Inter-radar interference analysis and concept of scalable fast chirp FMCW radar for automotive applications. In: 20th International Radar Symposium (IRS), pp. 1–8 (2019)
31. Uysal, F., Sanka, S.: Mitigation of automotive radar interference. In: IEEE Radar Conference (RadarConf18), pp. 0405–0410 (2018)
32. Alland, S., et al.: Interference in automotive radar systems: characteristics, mitigation techniques, and current and future research. IEEE Signal Process. Mag. 36(5), 45–59 (2019)
33. Norouzian, F., et al.: Phenomenology of automotive radar interference. IET Radar Sonar Navig. 15(9), 1045–1060 (2021)
34. Giannini, V., et al.: A 79 GHz phase-modulated 4 GHz-BW CW radar transmitter in 28 nm CMOS. IEEE J. Solid-State Circuits 49(12), 2925–2937 (2014)
35. Roos, F., et al.: Radar sensors for autonomous driving: modulation schemes and interference mitigation. IEEE Microw. Mag. 20(9), 58–72 (2019)
36. Overdevest, J., et al.: Uncorrelated interference in 79 GHz FMCW and PMCW automotive radar. In: 2019 20th International Radar Symposium (IRS), pp. 1–8 (2019)
37. He, Y., et al.: A deep-learning method for radar micro-Doppler spectrogram restoration. Sensors. 20(17), 5007 (2020)

How to cite this article: Kumbul, U., et al.: Automotive radar interference study for different radar waveform types. IET Radar Sonar Navig. 16(3), 564–577 (2022). https://doi.org/10.1049/rsn2.12203

APPENDIX A

A.1 | Derivatives of phase changes

In this proof we explain how the derivative of a code signal is taken with respect to time. It should be noted that in the derivation it is assumed that the phase term spans $\phi_n \in \{0, \pi\}$, since current COTS automotive radars only support BPSK phase shifting using the microcontrollers TEF810X and S32R274. If the phase term is a function of time, this must be taken into account during the derivation.

Recall that

$$\text{rect}\left(\frac{t-x}{y}\right) = u\left(t-x+\frac{y}{2}\right) - u\left(t-x-\frac{y}{2}\right), \quad \text{(A.1)}$$

and

$$\frac{d}{dt}\text{rect}\left(\frac{t-x}{y}\right) = \delta\left(t-x+\frac{y}{2}\right) - \delta\left(t-x-\frac{y}{2}\right), \quad \text{(A.2)}$$

where u is a unit step function and δ is a Dirac delta function. Similarly, the chip terms can be written as:

$$\begin{aligned}\phi_n \text{rect}&\left(\frac{t-\tau-(n-1/2)T_a}{T_a}\right)\\ &= \phi_n u\left(t-\tau-\left(n-\frac{1}{2}\right)T_a+\frac{T_a}{2}\right)\\ &\quad - \phi_n u\left(t-\tau-\left(n-\frac{1}{2}\right)T_a-\frac{T_a}{2}\right),\end{aligned} \quad \text{(A.3)}$$

and

$$\phi_{n+1}\mathrm{rect}\left(\frac{t-\tau-(n+1/2)T_a}{T_a}\right) = \phi_{n+1}u\left(t-\tau-\left(n+\frac{1}{2}\right)T_a+\frac{T_a}{2}\right) - \phi_{n+1}u\left(t-\tau-\left(n+\frac{1}{2}\right)T_a-\frac{T_a}{2}\right), \tag{A.4}$$

for the nth and $(n+1)$th elements, respectively. Then, take the derivative of Equations (A.3) and (A.4) with respect to time as:

$$\frac{d}{dt}\left(\phi_n\mathrm{rect}\left(\frac{t-\tau-(n-1/2)T_a}{T_a}\right)\right) = \phi_n\delta\left(t-\tau-\left(n-\frac{1}{2}\right)T_a+\frac{T_a}{2}\right) - \phi_n\delta\left(t-\tau-\left(n-\frac{1}{2}\right)T_a-\frac{T_a}{2}\right), \tag{A.5}$$

and

$$\frac{d}{dt}\left(\phi_{n+1}\mathrm{rect}\left(\frac{t-\tau-(n+1/2)T_a}{T_a}\right)\right) = \phi_{n+1}\delta\left(t-\tau-\left(n+\frac{1}{2}\right)T_a+\frac{T_a}{2}\right) - \phi_{n+1}\delta\left(t-\tau-\left(n+\frac{1}{2}\right)T_a-\frac{T_a}{2}\right), \tag{A.6}$$

for the nth and $(n+1)$th elements, respectively. To take the summation of derivatives, we have to consider a junction point in which the adjacent elements are linked. Thus, the relevant junction point includes the right part of the nth and left part of the $(n+1)$th elements, as shown below:

$$\phi_{n+1}\delta\left(t-\tau-\left(n+\frac{1}{2}\right)T_a+\frac{T_a}{2}\right) - \phi_n\delta\left(t-\tau-\left(n-\frac{1}{2}\right)T_a-\frac{T_a}{2}\right) = \phi_{n+1}\delta(t-\tau-nT_a)-\phi_n\delta(t-\tau-nT_a). \tag{A.7}$$

Therefore,

$$\frac{1}{2\pi}\frac{d}{dt}\phi_{tar_{code}}(t) = \frac{1}{2\pi}\frac{d}{dt}\sum_{n=1}^{L_a}\phi_n\mathrm{rect}\left(\frac{t-\tau-\left(n-\frac{1}{2}\right)T_a}{T_a}\right) = \frac{1}{2\pi}\sum_{n=1}^{L_a}\phi_{n+1}\delta(t-\tau-nT_a)-\phi_n\delta(t-\tau-nT_a) = \frac{1}{2\pi}\sum_{n=1}^{L_a}(\phi_{n+1}-\phi_n)\delta(t-\tau-nT_a), \tag{A.8}$$

and

$$\frac{1}{2\pi}\frac{d}{dt}\phi_{int_{code}}(t) = \frac{1}{2\pi}\frac{d}{dt}\sum_{n=1}^{L_b}\phi_n\mathrm{rect}\left(\frac{t-\tau_{int}-\left(n-\frac{1}{2}\right)T_b}{T_b}\right) = \frac{1}{2\pi}\sum_{n=1}^{L_b}\phi_{n+1}\delta(t-\tau_{int}-nT_b)-\phi_n\delta(t-\tau_{int}-nT_b) = \frac{1}{2\pi}\sum_{n=1}^{L_b}(\phi_{n+1}-\phi_n)\delta(t-\tau_{int}-nT_b). \tag{A.9}$$